Review

Sandip Ghosal

Department of Mechanical Engineering,
Northwestern University,
Evanston, IL, USA

Fluid mechanics of electroosmotic flow and its effect on band broadening in capillary electrophoresis

Electroosmotic flow (EOF) usually accompanies electrophoretic migration of charged species in capillary electrophoresis unless special precautions are taken to supress it. The presence of the EOF provides certain advantages in separations. It is an alternative to mechanical pumps, which are inefficient and difficult to build at small scales, for transporting reagents and analytes on microfluidic chips. The downside is that any imperfection that distorts the EOF profile reduces the separation efficiency. In this paper, the basic facts about EOF are reviewed from the perspective of fluid mechanics and its effect on separations in free solution capillary zone electrophoresis is discussed in the light of recent advances.

Keywords: Band broadening / Capillary electrophoresis / Electroosmosis / Lubrication theory / Review / Taylor dispersion
DOI 10.1002/elps.200305745

Contents

1 Introduction

Electroosmotic flow (EOF) was first reported by Reuss [1] in 1809 in experiments that demonstrated that water could be made to percolate through porous clay diaphragms through the application of an electric field. The observed mobility of water was due to the fact that the clay particles (and many other solid substrates such as glass, silicon, polymeric materials, minerals of various kinds, *etc.*) acquire a surface charge when in contact with an electrolyte. The immobile surface charge in turn attracts a cloud of free ions of the opposite sign creating a thin (∼1–10 nm under typical conditions, *e.g.*, univalent electrolyte at a concentration of 1–100 mol per m^3) Debye layer of mobile charges next to it. The thickness of this electric double layer (EDL) is determined by a balance between the intensity of thermal (Brownian) fluctuations and the strength of the electrostatic attraction to the substrate. In the presence of an external electric field, the fluid in this charged Debye layer acquires a momentum which is then transmitted to adjacent layers of fluid through the effect of viscosity. If the fluid phase is mobile (such as in a packed bed of particles or in a narrow capillary), it would cause the fluid to flow (electroosmosis). In a typical separation in capillary electrophoresis (CE)* both electroosmosis (sometimes also called electroendosmosis) and electrophoresis occur simultaneously. Therefore, the resultant migration velocity of each species '*i*' is

$$\mathbf{u}_{\text{total}}^{(i)} \equiv \mathbf{u}_{\text{eof}} + \mathbf{u}_{\text{eph}}^{(i)} \tag{1}$$

where the first term is the bulk EOF velocity and the second term is the migration velocity relative to still fluid of species *i* (generally different for each species). Due to

Correspondence: Dr. Sandip Ghosal, Department of Mechanical Engineering, Northwestern University, 2145 Sheridan Road, Evanston, IL 60208, USA
E-mail: s-ghosal@northwestern.edu
Fax: +847-491-3915

Abbreviations: EDL, electric double layer; **HS**, Helmholtz-Smoluchowski; **μ-TAS**, micro total analysis system

* In this paper CE will always refer to 'free solution capillary zone elecrophoresis', which is the only mode considered here, though the ideas presented could with appropriate modification be useful for other separation modes.

the thinness of the EDL (1–10 nm) compared to typical channel radii (10–100 μm), the electrical driving forces are localized in a thin sheath at the solid-fluid interface.

EOF can have a number of effects on the efficiency of separation. First note that if $|\mathbf{u}_{eof}| > \left|\mathbf{u}_{eph}^{(i)}\right|$ for all *i*, then all species move in the same direction enabling single point detection of charged species of either sign. If the capillary is uniformly charged and the inlet and outlet are at the same pressure, it is well-known that the flow is uniform throughout the capillary cross-section except for a very thin EDL near the wall where the flow velocity rapidly decreases from its free stream value to zero at the substrate/fluid interface [2]. This uniform velocity is given by the Helmholtz-Smoluchowski (HS) formula:

$$u_e = -\frac{\varepsilon E \zeta}{4\pi\mu} \tag{2}$$

where ε is the dielectric constant of the fluid, *E* is the applied electric field, ζ is the zeta-potential at the electrolyte/substrate interface, and μ is the fluid viscosity. Therefore, except in the thin EDL there is no shear in the flow. Thus, EOF does not add any significant shear induced axial dispersion (Taylor-Aris dispersion) to the analyte. Band broadening in this case is purely due to axial molecular diffusion.

Clearly, Eq. (2) cannot be valid if any of the parameters that enter into the expression vary in the axial direction, or, if the cross-section varies along the capillary. This is because any such variation would require the continuity condition, that the fluid flux through all cross-sections be the same to be violated. Axial variations usually lead to induced pressure gradients that drive a 'Poiseuille' type of flow*. Thus, the flat EOF profile becomes distorted resulting in strong band broadening due to Taylor-Aris dispersion [3, 4]. The effect of such axial variability is discussed in detail in this review.

The rest of this paper is organized in the following way: in the next section, the basic equations describing EOF in any conduit are presented. In Section 3, these basic equations are simplified by introducing the assumption of thin Debye layers. An exact solution of the EOF problem in cylindrical capillaries due to Rice and Whitehead is presented next (Section 4) and compared with the corresponding reduced solution in the case of infinitely thin Debye layers. In Section 5, the more difficult case of EOF through capillaries with axial inhomogeneities is considered and solutions are discussed for two special geometries. In order to handle problems involving inhomogeneous channels of arbitrary cross-sectional shapes, the potential flow and the lubrication approximation are introduced in Sections 5.2 and 5.3. Finally, the dispersive effects of EOF in homogeneous and inhomogeneous channels are considered in Section 6. A summary is presented in Section 7.

* Sometimes referred to in the literature as 'laminar flow'. However, this terminology is inconsistent with usage in fluid mechanics, since all flows of relevance in CE, including the 'pure' EOF are laminar (as opposed to turbulent) due to the smallness of the Reynolds numbers involved.

2 Electroosmotic flow

The equations describing the velocity field, **u**, of the fluid phase are those of momentum conservation:

$$\rho_0(\partial_t \mathbf{u} + \mathbf{u} \cdot \nabla \mathbf{u}) = -\nabla p + \mu \nabla^2 \mathbf{u} - \rho_e \nabla \phi \tag{3}$$

and continuity:

$$\nabla \cdot \mathbf{u} = 0 \tag{4}$$

where ρ_0 and μ are the (constant) density and viscosity of the fluid, *p* is the fluid pressure, φ is the electric potential, and the charge density in the EDL, ρ_e is related to the potential by Poisson's equation

$$\varepsilon \nabla^2 \phi = -4\pi\rho_e \tag{5}$$

To close the system, we need an equation for determining φ, which is the Poisson-Boltzmann equation

$$\nabla^2 \phi = -\kappa^2 \phi \tag{6}$$

where κ is a constant determined by the ionic composition of the electrolyte [5]. The Debye length is defined by $\lambda_D = 2\pi/\kappa$. The form (6) incorporates the Debye-Hückel approximation $\phi \ll k_B T/e$ where k_B is the Boltzmann constant, *T* is the absolute temperature, and *e* is the electronic charge. At room temperature, $k_B T/e \approx 25$ mV. The electric potential at the substrate buffer interface could be as high as 100 mV. Thus, the Debye-Hückel approximation is not always satisfied, in which case Eq. (6) should be replaced by the more accurate but nonlinear Gouy-Chapman form [5]. However, Eq. (6) is still useful for the purpose of qualitative understanding even in situations where it may not be strictly valid over the entire width of the EDL.

The boundary conditions are those of "no slip" for the fluid velocity at the solid-fluid interface:

$$\mathbf{u}|_{\text{solid surface}} = 0 \tag{7}$$

and

$$\phi|_{\text{solid surface}} = \zeta \tag{8}$$

where the potential at the solid fluid boundary, ζ, is specified. Due to the rapid change in the potential at the interface the definition of "at the interface" is somewhat ambiguous. It is believed that the solid substrate usually

has a layer of adsorbed immobile ions next to it known as the Stern layer. It is the ions in the fluid phase adjoining the Stern layer that are mobile and the distribution of which are governed by the Debye-Hückel or more generally the Gouy-Chapman theory. The outer edge of the Stern layer is therefore identified as the "slip plane" where the no-slip boundary condition is applied [2]. The "zeta-potential" ζ is defined as the electric potential at this slip plane and is assumed known for the purpose of this paper. The applied electric field is assumed to distort the structure of the EDL by a negligible amount. Clearly, this would be true if $V/L \ll \zeta/\lambda_D$ where V is the applied voltage over a segment L of the capillary. Using typical values $\zeta \sim 100$ mV and $\lambda_D \sim 10$ nm, we find that $\zeta/\lambda_D \sim 10^5$ V/cm $\gg V/L \sim$300 V/cm.

The ratio of the characteristic magnitude of the left hand side to the right hand side of Eq. (3) is measured by the (dimensionless parameter) Reynolds number, $Re = (a_0\rho_0 u_e/\mu)$ where a_0 is a characteristic radius and u_e is a characteristic electroosmotic speed. Estimates using typical values for microfluidic applications give $Re \sim 0.001$–1.0, so that the left hand side can often be ignored (in that case Eq. (3) becomes the Stokes equation), or at least treated as a small correction. Unlike applications of fluid mechanics to large-scale phenomena where the left hand side is dominant leading to instabilities and turbulence, microfluidics is always characterized by smooth laminar flow.

3 The thin EDL limit

The theory of electrophoretic motion of charged particles of characteristic size 'a' has been well studied in the limit of thick ($\lambda_D \gg a$) as well as thin ($\lambda_D \ll a$) Debye layers. However, since the characteristic radius of microfluidic channels $\sim$10–100 μm, whereas, the Debye length $\lambda_D \sim$ 1–10 nm, the thin Debye layer approximation is usually an excellent one for the purpose of studying EOF, at least for the majority of current microfluidic applications. In the limit of thin EDL, the Navier-Stokes/Poisson-Boltzmann system described in the last section may be replaced by a simpler set of equations. The EDL then forms a very thin boundary layer at the solid fluid interface where the electrical forces are confined.

At leading order, the dominant balance is between the viscous and the electrical forces in the boundary layer:

$$\mu \frac{\partial^2 u}{\partial z^2} + \rho_e E \cong 0 \tag{9}$$

where E is the external electric field which is in the tangential direction. Since rates of change across the boundary layer (z-axis) are much larger than along it (x-axis), Poisson's Eq. (5) may be written as

$$\rho_e \cong -\frac{\varepsilon}{4\pi}\frac{\partial^2 \phi}{\partial z^2} \tag{10}$$

On eliminating ρ_e between Eqs. (9) and (10), integrating the resulting differential equation and using the boundary conditions at the inner and outer edges of the EDL, the following jump condition across the EDL is derived

$$\mathbf{u} - \mathbf{u}_{solid} \equiv \Delta \mathbf{u} = -\frac{\varepsilon \mathbf{E} \zeta}{4\pi\mu} \tag{11}$$

where in Eq. (11), $\mathbf{u}_{solid}$ is the velocity of the solid at a point on the solid-fluid interface and $\mathbf{u}$ is the velocity of the fluid at the corresponding point, just above the (infinitely thin) Debye layer. A formal asymptotic development in terms of the small parameter λ_D/a_0 (where a_0 is a characteristic radius) has been presented by Anderson [6]. Equation (11) is known as the Helmholtz-Smoluchowski (HS) slip boundary condition after the pioneering work of Helmholtz [7] and Smoluchowski [8]. Thus, in the limit of thin Debye layers the term $-\rho_e \nabla\phi$ may be dropped from Eq. (3), instead at the boundary, the no-slip boundary condition (7) is replaced by (11). Since the external field $\mathbf{E}$ is tangential to the interface, (11) implies that the normal component of the velocity is continuous. Thus, the equations of fluid flow inside the capillary become exactly identical to the classical fluid flow equations, the coupling to the electrical problem is only felt through the boundary condition in Eq. (11).

4 EOF in a uniform cylindrical capillary

In capillary zone electrophoresis (CZE) EOF takes place in narrow cylindrical capillaries that to a first approximation can be considered to be infinitely long and uniformly charged. Under those conditions, the Debye-Hückel form of the Poisson-Boltzmann equation admits an exact solution [9]:

$$\phi = \zeta \frac{I_0(\kappa r)}{I_0(\kappa a)} \tag{12}$$

where I_0 is the zeroth order modified Bessel's function of the first kind, r is the distance from the axis, and a is the internal radius of the capillary. Equation (5) can then be used to determine the charge density. Further, substitution of ρ_e in the Navier-Stokes Eq. (3), results in an equation that may be integrated exactly to determine the flow profile $u(r)$. In the absence of an imposed pressure gradient, the solution, after Rice and Whitehead [9], is

$$u(r) = -\frac{\varepsilon \zeta E}{4\pi\mu}\left[1 - \frac{I_0(\kappa r)}{I_0(\kappa a)}\right] \tag{13}$$

Since the fluid flow equation is linear in this limit, clearly a pressure-driven flow can be added to the solution (superposition) in the event that both a pressure gradient and an electric field are simultaneously applied.

In the thin EDL limit, the flow problem can be formulated in terms of the HS slip boundary conditions. Due to symmetry in the axial direction, the Navier-Stokes equation simply reduces to

$$\frac{\mu}{r}\frac{d}{dr}\left(r\frac{du}{dr}\right) = 0 \tag{14}$$

with the 'slip' boundary conditions

$$u(r=a) = -\frac{\varepsilon\zeta E}{4\pi\mu} \tag{15}$$

The only solution, without a singularity at the origin, is the 'plug flow' profile

$$u(r) = u(r=a) = -\frac{\varepsilon\zeta E}{4\pi\mu} \tag{16}$$

Equation (16) may be compared to the Rice-Whitehead solution (13). When $\kappa a \gg 1$ (thin EDL limit) [10]

$$I_0(z) \sim \frac{\exp z}{\sqrt{2\pi z}}\left[1+\frac{1}{8z}+\cdots\right] \tag{17}$$

therefore the term $I_0(\kappa r)/I_0(\kappa a)$ in Eq. (13) is negligible unless $r \approx a$. Near $r = a$ we have $I_0(\kappa r)/I_0(\kappa a) \sim \exp[-\kappa(a-r)]$, thus the HS solution (16) is recovered except in a thin boundary layer $a-r \sim \kappa^{-1} \sim \lambda_D$ within which the velocity drops precipitously to zero in order to satisfy the no-slip boundary condition at $r = a$. This behavior is shown in Fig. 1. Exact solutions within the Debye-Hückel approximation are also available for EOF between parallel plates for any Debye length [11]. They show a similar 'boundary layer' type of behavior.

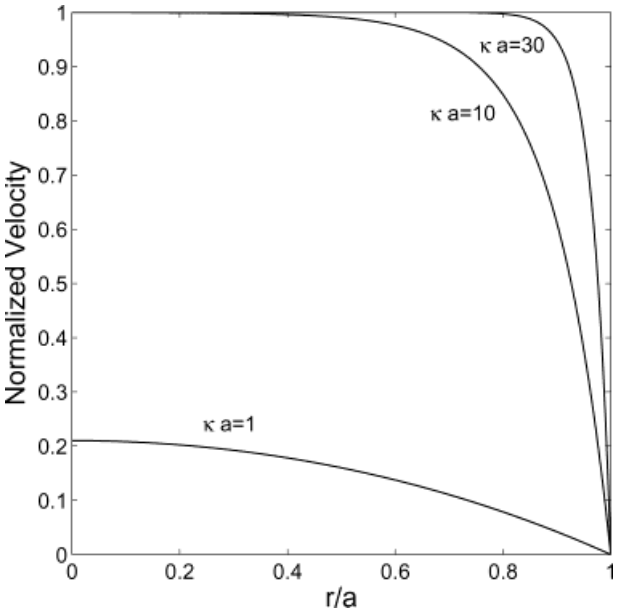

Figure 1. Normalized velocity profile from the Rice-Whitehead solution showing the thin boundary layer at the wall for small Debye lengths.

In the case of CE channels etched on substrates for micrototal analysis system (μ-TAS) applications, the channels are usually rectangular or trapezoidal rather than circular in cross-section. However, in the thin EDL limit the plug flow profile is valid for channels of arbitrary cross-sectional shape since it simultaneously solves the Stokes flow equation and satisfies the HS slip boundary condition. This is of course not true in the case of finite EDL thickness as the detailed structure of the flow within the EDL is determined by the cross-sectional geometry of the capillary.

5 Axially inhomogeneous channels

We have seen so far, that except for a very thin sheath around the channel walls, EOF has a uniform flow profile. This is a great advantage in CE applications since it implies that the presence of EOF does not lead to significant added dispersion. This conclusion, however, is valid as long as all of the parameters involved, namely the electric field **E**, dielectric constant ε, the zeta-potential ζ and viscosity μ are constants. Variability in any of these parameters could induce axial pressure gradients which perturb the flow and distort the uniformity of the flow profile. Calculating the perturbations in the flow due to such causes and the resultant axial dispersion is a fundamental fluid mechanics problem of considerable interest in CE.

5.1 Exactly solvable models

Anderson and Idol [12] considered the problem of EOF through a uniform, infinite, straight cylindrical capillary with a ζ-potential that varies solely in the axial direction, $\zeta = \zeta(x)$. A uniform external electric field and zero imposed pressure gradient were assumed. An exact solution to the Stokes flow problem was derived under the assumption of thin EDL. It was shown that the velocity field $\mathbf{u} = u\hat{\mathbf{x}} + \hat{\mathbf{r}}v$ may be expressed in terms of the stream function ψ,

$$u = -\frac{1}{r}\frac{\partial\psi}{\partial r} \tag{18}$$

$$v = -\frac{1}{r}\frac{\partial\psi}{\partial x} \tag{19}$$

where ψ is given by a series expansion

$$\psi = \frac{\varepsilon E}{4\pi\mu}\left[\frac{r^2}{2}\langle\zeta\rangle - 2\sum_{m=1}^{\infty} a_m^c(r)\cos\left(\frac{2m\pi x}{L}\right) - \right.$$
$$\left. - 2\sum_{m=1}^{\infty} a_m^s(r)\sin\left(\frac{2m\pi x}{L}\right)\right] \quad (20)$$

where

$$\frac{a_m^c}{\hat{\zeta}_m^c} = \frac{a_m^s}{\hat{\zeta}_m^s} = \frac{rI_0(\alpha_m)I_1(\alpha_m r) - r^2 I_0(\alpha_m r)I_1(\alpha_m)}{\alpha_m I_1^2(\alpha_m) + 2I_0(\alpha_m)I_1(\alpha_m) - \alpha_m I_0^2(\alpha_m)} \quad (21)$$

and

$$\hat{\zeta}_m^c = \frac{1}{L}\int_0^L \zeta(x)\cos\left(\frac{2m\pi x}{L}\right)dx \quad (22)$$

$$\hat{\zeta}_m^s = \frac{1}{L}\int_0^L \zeta(x)\sin\left(\frac{2m\pi x}{L}\right)dx \quad (23)$$

are the cosine and sine transform of the ζ-potential $\zeta(x)$, $\alpha_m = 2m\pi/L$, and $\langle\ \rangle$ indicates the average over the length of the capillary:

$$\langle f\rangle = \frac{1}{L}\int_0^L f dx \quad (24)$$

In Eq. (21), I_n denotes the modified Bessel function of integer order n.

The above solution implies a remarkably simple formula for the cross-sectional average of the axial velocity, $\bar{u}$ (or equivalently, the volume flux per unit cross-sectional area),

$$\bar{u} = -\frac{\varepsilon\langle\zeta\rangle E}{4\pi\mu} \quad (25)$$

which follows on integrating Eq. (18) over the cross-section of the capillary. Thus, the flux per unit area at any instant over any cross-section is the same and equal to that of the flow through a uniform capillary with $\zeta = \langle\zeta\rangle$.

Ajdari [13] considered the problem of EOF between a pair of parallel plates at $z = \pm h$ under the application of a uniform external electric field, E, and arbitrary position dependent variations of the zeta-potential on the surface of the plates $\zeta = \zeta_{\pm}(x, y)$. Though the parallel plate geometry is not directly relevant to CE applications, it may serve as a reasonable approximation to flow in shallow rectangular channels etched on chips. The analysis is based on the assumptions of low zeta-potentials ($\zeta \ll k_B T$, the Debye-Hückel approximation) and low Reynolds numbers (Stokes flow). On account of the linearity of the fluid flow equations in the Stokes flow limit, and, since the problem for the potential in the EDL is decoupled from the fluid problem, an exact solution could be obtained by Fourier transforming the equations along the planes parallel to the plates. In a subsequent paper [14], Ajdari generalized the solution to include the effect of small (compared to plate separation) amplitude irregularities on the surface of the plates.

Ajdari's solutions illustrate some interesting features of EOF such as the presence of recirculating regions which could be useful in the design of microfluidic mixers. In fact, Stroock *et al.* [15] constructed such mixers using EOF in a long channel of rectangular cross-section (260 μm $\times$ 130 μm) with a patterned surface charge of alternating sign that was fabricated using soft lithographic techniques [16]. It is further shown by Ajdari that surface irregularities and variations in the zeta-potential in combination could generate net forces on the plates which could even be perpendicular to the applied electric field and need not vanish even if the net charge on either plate vanishes. The framework of Ajdari was applied by Long *et al.* [17] to obtain analytical solutions in the neighborhood of localized 'defects' in the zeta-potential for both the parallel plate as well as cylindrical geometries. These solutions are useful in providing an understanding of the perturbations in EOF that may result from various local surface imperfections of the zeta-potential likely in any practical device.

5.2 Potential flow solution

Let us consider the problem of EOF in a conduit of arbitrary geometry but in the thin EDL approximation. Further, assume that all fluid and material properties are uniform and that no external pressure gradient has been applied across the capillary. Let us denote by S the walls of the conduit and by S_0 and S_1 the equipotential surfaces $\phi = \phi_0$ and $\phi = \phi_1$, respectively, near the inlet and outlet sections. These are the potentials of the reservoirs at the extremities of the capillary. Then it follows by direct calculation that

$$\mathbf{u} = \frac{\varepsilon\zeta}{4\pi\mu}\nabla\phi \quad (26)$$

where ϕ is a solution of the boundary value problem

$$\nabla^2\phi = 0; \quad \phi = \zeta \text{ on } S,\ \phi_0 \text{ on } S_0, \text{ \& } \phi_1 \text{ on } S_1 \quad (27)$$

has the following properties

$$\nabla\cdot\mathbf{u} = 0, \quad \nabla^2\mathbf{u} = 0 \quad (28)$$

Further, $\mathbf{u}$ satisfies the HS slip boundary conditions (Eq. 11). Thus, Eq. (26) is already the solution of the problem of EOF through the conduit in the Stokes flow limit.

If the Reynolds number *Re* is not necessarily negligible but the flow is known to be steady and irrotational, then the Navier-Stokes Eqs. (3) and (4) outside the EDL may be replaced by

$$\nabla \times \mathbf{u} = 0; \quad \nabla \cdot \mathbf{u} = 0 \tag{29}$$

Once again, we see that Eq. (26) automatically satisfies these equations and is therefore the unique solution to the hydrodynamic problem.

The existence of this "similitude" between the electroosmotic velocity **u** and the electric field $-\nabla\phi$ was first pointed out by Cummings *et al.* [18]. When the conditions needed for such similitude are satisfied, Eq. (26) provides a remarkably simple solution to the problem of determining the EOF since one only needs to solve the Dirichlet problem for the potential and a wide variety of analytical and numerical techniques exist for this task. It should also be clear that if the prefactor multiplying $\nabla\phi$ in Eq. (26) fails to be a constant, then **u** does not satisfy either the continuity equation or the equation for the conservation of momentum and Eq. (26) therefore is no longer a solution. It is this class of problems that we consider next.

5.3 Lubrication approximation

When the HS slip velocity is variable over the capillary surface, an analytical solution for the flow field is difficult except for the special geometries discussed in the last section. Generally one may need to resort to the more expensive process of full numerical simulation. However, if the variations are 'slow' in the axial direction; a term that will be made more precise later, the technique of lubrication theory [19] permits analytical solutions to be obtained even for channels with complicated geometrical shapes. Lubrication theory was originally developed to analyze the motion of lubricants in the narrow gap between machine parts (and hence the name). It has since found wide application in various areas of fluid mechanics, such as in the analysis of blood flow in very narrow capillaries [20, 21]. It has recently been applied to the problem of EOF by Ghosal [22] in the context of the thin EDL limit.

The theory is based on the following assumptions: (i) The characteristic length scale for the variation of the cross-sectional shape and area in the axial (x) direction of the channel is very much larger than a characteristic radius (a_0). (ii) The characteristic length scale for the variation of the slip velocity in the x direction is very much larger than a_0. (iii) The characteristic time-scale (T) for any temporal variations is very much larger than the diffusion scale ($t_d \equiv a_0^2/\nu$) (ν being the kinematic viscosity of the fluid).

If the assumption of slow variations as defined above is satisfied, then a formal asymptotic solution to the problem of EOF in terms of the ratio of characteristic radial distance to characteristic axial scale (a small parameter) may be carried out [22] and the solution may be summarized as follows: $\mathbf{u} \sim \hat{\imath}\, u\,(x, y, z) + O\,(\epsilon)$, $\mathbf{E} \sim \hat{\imath}\, E\,(x) + O\,(\epsilon)$,

$$u = -\frac{u_p}{\mu}\frac{dp}{dx} + \frac{\varepsilon F}{4\pi\mu}\frac{\psi}{A(x)} \tag{30}$$

$$Q = -\frac{\bar{u}_p}{\mu}A(x)\frac{dp}{dx} + \frac{\varepsilon F\bar{\psi}}{4\pi\mu} \tag{31}$$

$$E(x) = F/A(x) \tag{32}$$

Here, F is a constant representing the electric flux through any cross-section, $A(x)$ is the cross-sectional area and the overbar indicates average over the cross-section, $\bar{f} = A^{-1}\int f\, dydz$. The constant Q represents the volume flux of fluid through any cross-section. The functions u_p, defined by $\nabla^2 u_p = 0$ and $u_p|_{\partial D(x)} = 0$ and the function ψ defined by $\nabla^2\psi = 0$ and $\psi|_{\partial D(x)} = -\zeta$ are properties of the channel geometry and charge distribution alone. They are defined on the domain $D(x)$ representing the cross-section of the channel with boundary ∂D at axial location 'x'. Both of these functions u_p and ψ may be evaluated by quadrature from a knowledge of the Green function, G, of the Laplace operator with zero boundary condition corresponding to the domain $D(x)$:

$$u_p = \frac{1}{4\pi}\int_{D(x)} G(x; y, z, y_*, z_*)\,dy_*\,dz_*$$

$$\psi = \frac{1}{4\pi}\oint_{\partial D(x)} \zeta(x, y_*, z_*)\left(m\frac{\partial G}{\partial y_*} + n\frac{\partial G}{\partial z_*}\right)ds_* \tag{33}$$

where (m, n) are the direction cosines of the unit normal on $\partial D(x)$.

According to Eqs. (30)–(32), the flow velocity in the axial direction in a slowly varying channel is a linear superposition of a purely pressure-driven flow, and a pure EOF. The axial pressure pressure gradient and electric field are calculated by using the dual conditions: (a) the fluid is incompressible, (b) the electric flux must obey the Gauss law. The solution is completely specified by two independent physical constants, the volume flux of fluid, Q, and, the electric flux, F. These constants may be expressed, if desired, in terms of the total pressure drop, and, the total voltage drop, respectively, between the inlet and outlet sections, which yields the following generalization of Poiseuille's law:

$$Q = \frac{p_a - p_b}{8\mu L}\pi a_*^4 - \frac{\varepsilon\zeta_*}{4\pi\mu}\pi a_*^2\frac{V_a - V_b}{L} \tag{34}$$

Here, $p_a - p_b$ is an applied pressure drop and $V_a - V_b$ is an applied voltage drop along a length L of the capillary. The constants a_* and ζ_* may be regarded as "effective" values

for the radius and the ζ-potential, respectively, and they are defined as

$$a_* = \left[\frac{8}{\pi\left\langle \bar{u}_p^{-1}A^{-1}\right\rangle}\right]^{1/4}$$

$$\zeta_* = -\frac{1}{\sqrt{8\pi}}\frac{\left\langle \bar{\psi}\bar{u}_p^{-1}A^{-1}\right\rangle}{\left\langle A^{-1}\right\rangle\left\langle \bar{u}_p^{-1}A^{-1}\right\rangle^{1/2}} \tag{35}$$

Here, the parameter a_* is determined solely by channel geometry and ζ_* is determined solely by the channel geometry and the nature of the distribution of the ζ-potential.

It is instructive to compare the lubrication theory result with the exact solution of the problem of EOF in a uniform cylindrical capillary with inhomogeneous charge distribution solved by Anderson and Idol [12], also in the thin EDL limit. For a uniform cylindrical capillary (radius a_0) with ζ varying only in the x direction Eq. (35) implies $\zeta_* = \langle\zeta\rangle$ which is the same as the result derived by Anderson and Idol and discussed earlier. For a sinusoidally varying wall charge,

$$\zeta(x) = \zeta_0 + \Delta\zeta\,\sin(2\pi x/\lambda) \tag{36}$$

Then Anderson and Idol's result implies:

$$\frac{u}{u_0} = 1 + \frac{\Delta\zeta}{\zeta_0}F(\rho)\sin(\alpha X) \tag{37}$$

where

$$F(\rho) = \frac{\alpha^{-1}I_0(\alpha\rho)\left[1 - \dfrac{\alpha I_0(\alpha)}{2I_1(\alpha)}\right] + \dfrac{\rho}{2}I_1(\alpha\rho)}{\alpha^{-1}I_0(\alpha) + \dfrac{1}{2}I_1(\alpha) - \dfrac{I_0^2(\alpha)}{2I_1(\alpha)}} \tag{38}$$

$\rho = r/a_0$, $X = x/a_0$, $u_0 = -\varepsilon E\zeta_0/(4\pi\mu)$ and $\alpha = 2\pi(a_0/\lambda)$. This may be compared with our solution which is Eq. (37) but with $F_0(\rho)$ instead of $F(\rho)$ where

$$F_0(\rho) = 2\rho^2 - 1 \tag{39}$$

Clearly $F(\rho) \sim F_0(\rho)$ in the limit $\alpha \ll 1$ (the lubrication limit). Figure 2 compares $F(\rho)$ and $F_0(\rho)$ for several values of the ratio a_0/λ. It is seen, that, for $a_0/\lambda \ll 1$ (in practice 0.1 or less), the prediction of the lubrication analysis is in excellent accord with the exact solution as expected. For $a_0/\lambda \sim 1$, the exact solution deviates significantly from the lubrication solution. In the opposite limit of $a_0/\lambda \gg 1$, the frequent reversal of the electric force results in no net transfer of momentum to the interior of the fluid, and the lubrication limit solution is qualitatively incorrect. The latter situation may describe random fine scale inhomogeneities in the wall charge of the type considered by Ajdari [13].

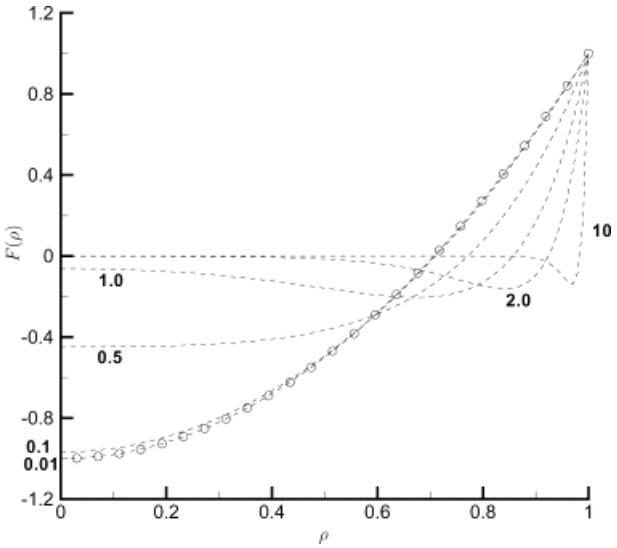

Figure 2. Comparison of the asymptotic solution in the lubrication limit (symbols) with the exact solution (dashed lines) according to Anderson and Idol for a_0/λ = 10.0, 2.0, 1.0, 0.5, 0.1, and 0.01. The asymptotic solution corresponds to $a_0/\lambda \to 0$. An infinitely thin EDL is assumed for both solutions.

6 Dispersion and EOF

The resolving power in CE is limited by axial dispersion of the analyte. The minimum resolvable difference in mobility $\Delta\mu \sim \bar{\mu}N$ where $\bar{\mu}$ is the average mobility of the two species and 'N' is the number of theoretical plates (square of the separation length divided by the variance of the concentration peak). Unlike a classical pressure-driven flow, which has a parabolic profile, EOF has an essentially flat profile (except in a thin EDL near the walls). Thus, under ideal circumstances, EOF should not contribute significantly to shear-induced axial dispersion (Taylor-Aris dispersion) so that essentially "diffusion limited" separation, where resolution is limited only by molecular diffusion is potentially realizable. However, in practice, various inhomogeneities can perturb the ideal EOF leading to significant band broadening. The important ones among such processes are discussed in the subsequent sections (also see the two reviews by Gaš and Kenndler [23] and by Gaš, Štědrý, and Kenndler [24]).

6.1 Dispersion due to finite size of the EDL

We have seen that in the thin EDL limit and in the absence of axial inhomogeneities, the dispersion is essentially due to molecular diffusion alone. However, the contribution of the zone of shear in the EDL can easily be estimated by actually calculating the Taylor-Aris dispersion coefficient

for the EOF profile derived by Rice and Whitehead presented in Section 4. This has been done by Datta and Kotamarthi [25] for a uniform infinitely long capillary. The same result was arrived at by Griffiths and Nilson [26] by a different method and also by McEldoon and Datta [27] in the more general case where the solute could interact with the wall. Subsequently, Griffiths and Nilson [28] extended the analysis to the case where the ζ-potential need not be small, and therefore the Debye-Hückel approximation cannot be made. However, in that case most of the calculations must be done numerically. Štědrý *et al.* [29] replaced the actual velocity profile by the combination of a plug flow region in the core and a stationary annular region near the wall and obtained a simplified expression for the plate height which depends on the thickness of the stationary zone. The evaluation of this thickness requires a numerical integration of the Poisson-Boltzmann equation.

Within the Debye-Hückel theory, the effective axial diffusion coefficient is given by [25]

$$\frac{\mathscr{D}}{D} = 1 + Pe^2 X_e(\phi)(1-\nu)^2 \tag{40}$$

where $Pe = \bar{u}a_0/D$ is a Peclet number based on the molecular diffusion coefficient, D, capillary radius a_0 and bulk flow velocity (volume flux per unit cross-section) $\bar{u}$;

$$\bar{u} = u_e(1-\eta) \tag{41}$$

where $u_e = -(\varepsilon\zeta E)/(4\pi\mu)$ and the parameter η is a measure of the reduction of the flow due to the presence of the double layer. It can be shown that

$$\eta = \frac{2}{\phi}\frac{I_1(\phi)}{I_0(\phi)} \tag{42}$$

where I_0 and I_1 are modified Bessel's functions of order zero and one, and $\phi = a_0/\lambda_D$ (λ_D is the Debye length). The function X_e is defined as

$$X_e(\phi) = \frac{\eta^2}{(1-\eta)^2}\left[\frac{3}{8} + \frac{2}{\phi^2} - \frac{1}{\eta\phi^2} - \frac{1}{\eta^2\phi^2}\right] \tag{43}$$

The parameter ν is zero for a pure EOF. However, if a pressure drop is applied across the capillary in addition to an electric voltage, ν is defined as the ratio of volume flux due to the pressure drop alone to that of the volume flux due to the voltage drop alone. It could have a negative sign if these two external influences on their own would drive a flux in opposite directions.

Typical Debye lengths in microfluidic applications are $\lambda_D \sim 1-10$ nm and typical radii are $a_0 \sim 10-100$ μm. Thus, $\phi \sim 10^3 - 10^5$. Using the asymptotic form for large ϕ, we have $\eta \approx 2/\phi \sim 10^{-5} - 10^{-3}$. Therefore, $\bar{u}$ differs from u_e by 0.1% or less. In typical CZE applications it is easily estimated that $Pe \sim 10-100$ for small to moderate sized molecules. From Eq. (43), $X_e \sim 10^{-10} - 10^{-6}$, so that $\mathscr{D}/D - 1 \sim 0.01$ or smaller. Thus, for such analytes the finiteness of the EDL usually has an insignificant effect and the dispersion is essentially limited by molecular diffusion, unless axial inhomogenieties drastically reduce performance. This conclusion may not be true if in the future channel radii become very much narrower (in the sub-μm range) for microfluidic applications. Further, for very large macromolecules, such as proteins, the diffusion coefficient can be $\sim 10-100$ times smaller so that the $Pe \sim 10^2 - 10^4$, in which case $\mathscr{D}/D - 1 \gg 1$ and the finiteness of the EDL could be important.

6.2 Dispersion due to analyte-wall interactions

An important source of dispersion in the analysis of cationic proteins is the variation in wall zeta-potential that results from the tendency of charged species to stick to the capillary walls [30]. This alters the ζ-potential in a nonhomogeneous and time-dependent manner inducing a pressure gradient that alters the flow profile as well as the bulk flow rate [31]. Highly asymmetric and broadened peaks are symptomatic of the presence of wall adsorption. The combination of loss of sample and enhanced dispersion can lead to reduction of the peak concentration in the sample below the detection threshold, in which case no peak at all is discernible in the detector response. Various strategies have been explored to overcome the problem of adsorption [32], however, in this paper we only review work related to the fluid mechanical processes at play.

The basic equations are those of fluid flow and scalar dispersion with a loss term, $f(c_w, s)$ which depends on the concentration at the wall, $c_w = c(a, x, t)$ and the concentration of adsorbed solute per unit area of the wall, s. A simple and commonly used wall interaction model is the Langmuir law:

$$f(c_w, s) = k_a c_w (s_m - s) - k_d s \tag{44}$$

where k_a and k_d, respectively, are adsorption and desorption coefficients and $s = s_m$ is the saturation concentration, the maximum solute concentration that the wall can hold. The ζ-potential in general is a function of the adsorbed concentration and could potentially also depend explicitly on x and t:

$$\zeta = g(s(x, t); x, t) \tag{45}$$

The form of g is determined by the structure of the EDL. If adsorption is assumed to simply alter the density of fixed charges at the wall and the Debye-Hückel approximation is assumed it is readily shown that

$$g = \zeta_0 - (2\pi\lambda_D zF/\varepsilon)\, s \tag{46}$$

where λ_D is the Debye length, F is the Faraday constant, z is the ionization state (number of fundamental charges per molecule), and s is assumed to be in units of moles per unit area.

Early works on this problem are due to Gaš *et al.* [33] and Štědrý *et al.* [34]. Though their analyses take account of the fact that analyte is lost to the wall, the consequent modification of the ζ-potential and therefore the hydrodynamic flow field were neglected. Indeed, the hydrodynamics was restricted to the trivial case of uniform flow at constant velocity independent of the adsorption process. Analysis of similar 'purely kinematic' models that neglect the perturbation in the hydrodynamic field have also been presented by other authors (see [35–37]). A detailed experimental study of wall adsorption and its consequences for the underlying EOF and dispersion is due to Towns and Regnier [38]. These experiments as well as others [39] together with their interpretation using simple fluid mechanical models [40, 41] indicate, that, the modification of the ζ-potential by adsorption, and the consequent perturbation of the hydrodynamic field, is an important, if not the principal cause of dispersion in these systems.

At distances large compared to a_0Pe (Pe is the Peclet number based on the EOF speed in the unmodified capillary) from the injection point, axial diffusion ensures that the analyte concentration is slowly varying in the axial direction relative to a length scale defined by the capillary radius a_0. In this limit, the lubrication theory discussed earlier can be extended to include a diffusing solute. The following one-dimensional coupled partial differential equations for the cross-sectionally averaged concentration $\bar{c}(x, t)$ and adsorbed concentration, $s(x, t)$ have been derived by Ghosal using asymptotic theory [31]:

$$\frac{\partial \bar{c}}{\partial t} + (\bar{u} + u_{ep})\frac{\partial \bar{c}}{\partial x} + \frac{a_0}{12D}\left[\frac{\partial}{\partial x}(u_*\bar{f}) + u_*\bar{f}_1\frac{\partial \bar{c}}{\partial x}\right] =$$

$$= \frac{\partial}{\partial x}\left(\mathscr{D}\frac{\partial \bar{c}}{\partial x}\right) - \frac{2}{a_o}\mathscr{S} \tag{47}$$

and

$$\frac{\partial s}{\partial t} = \mathscr{S} \tag{48}$$

where for convenience

$$u_* \equiv \bar{u} + \frac{\varepsilon E\zeta}{4\pi\mu} = \frac{\Delta p a_0^2}{8\mu L} + \frac{\varepsilon\zeta' E}{4\pi\mu} \tag{49}$$

with $\zeta' = \zeta - \langle\zeta\rangle$ and given pressure drop Δp across the capillary. The effective axial diffusivity and source terms are

$$\mathscr{D} = D + \frac{a_0^2 u_*^2}{48D} \tag{50}$$

$$\mathscr{S} = \bar{f}\left[1 - \frac{a_o}{4D}\bar{f}_1\right] \tag{51}$$

where

$$\bar{f} = f(\bar{c}, s) \quad \bar{f}_1 = \left.\frac{\partial f}{\partial c_w}\right|_{c_w=\bar{c}} \tag{52}$$

The sample concentration, $c(r, x, t)$ itself may be expressed as

$$c(r,x,t) = \bar{c}(x,t) + \frac{a_0^2 - 2r^2}{4a_0 D}\frac{\partial s}{\partial t} - \frac{2a_0^4 - 6a_0^2 r^2 + 3r^4}{24a_0^2 D}u_*\frac{\partial \bar{c}}{\partial x} \tag{53}$$

where the second and third terms are small corrections to the first.

According to Eq. (47) the mean concentration profile is advected at the bulk flow speed plus any electrophoretic migration speed if present, while simultaneously diffusing with an 'effective' axial diffusion coefficient shown in Eq. (50). This axial dispersion coefficient is precisely the classical Taylor-Aris dispersion coefficient calculated with that part of the flow field that is proportional to the induced pressure gradient. The last term represents losses to the wall after accounting for a small correction caused by the fact that the concentration at the wall differs by a small amount from the mean concentration $\bar{c}$.

In order to check the accuracy of the asymptotic theory, the complete set of coupled fluid flow and scalar equation for concentration was solved numerically assuming a thin EDL (*via* the HS slip boundary conditions) and Stokes flow. Periodic boundary conditions were assumed in the x (axial) direction. As initial conditions we used a trapezoidal profile for $c(r, x, 0) = c_0(x)$ approximately 10 radii wide and used a reasonable [42] set of parameter values shown in Table 1. Note that all parameters are in dimensionless units. Figure 3 shows the distribution of $\bar{c}/c_m$ (where c_m is the maximum concentration) and ζ/ζ_0 at the

Table 1. Parameter values for simulation

Parameter	L/a_0	Re	Pe	$k_a s_m/u_e$	$a_0 k_d/u_e$	s_m
Definition		a_0u_e/ν	a_0u_e/D			
Value	1000	0	100	0.1	0.0005	0.01

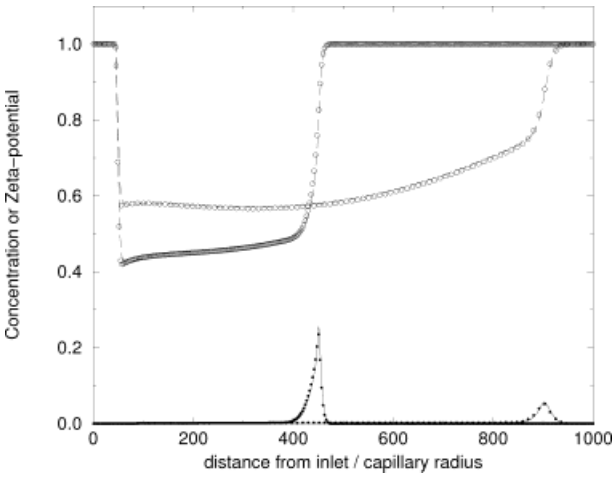

Figure 3. Comparison of asymptotic theory (symbols) with numerical simulation (lines) of the cross-sectionally averaged analyte concentration (lower curves) and ζ-potential (upper curves) at two time instants. The parameters are as in Table 1.

instant when the concentration peak arrives at a hypothetical detector placed at a distance x_d from the inlet. The figure shows two independent sets of results for $x_d = 450a_0$ and $x_d = 900a_0$. It is seen that as the sample moves down the capillary, the peak height decreases, the peak width increases and the peak shape becomes markedly asymmetric. The peak shapes have a striking qualitative similarity with observed CZE signals in an uncoated capillary for cationic proteins (see, *e.g.*, Fig. 8 of [38] and Fig. 10 of [43].) The ζ-potential is reduced behind the peak, however, with passage of time, the ζ-potential at a fixed position undergoes a gradual recovery. This is due to desorption from the capillary walls. For both $\bar{c}$ and ζ the simulation is seen to be in excellent agreement with the theoretical calculation using the 1-D equations.

In the case of a pure pressure-driven flow ($E = 0$ but $\Delta p > 0$), our problem reduces to the classical chromatographic problem first studied by Golay [44] and later refined by Aris [45] and others [46, 47]. If we linearize f by assuming $s \ll s_m$ and neglect desorption, $k_d = 0$ then we can rewrite Eq. (47) as

$$\frac{\partial \bar{c}}{\partial t} + (\tilde{u} + u_{ep})\frac{\partial \bar{c}}{\partial x} = \frac{\partial}{\partial x}\left(D\frac{\partial \bar{c}}{\partial x}\right) - \frac{2}{a_0}\mathscr{S} \tag{54}$$

where

$$\tilde{u} = \bar{u}\left[1 + \frac{a_0 k_a s_m}{6D}\right] \tag{55}$$

Thus, in this case, the profile of $\bar{c}$ is advected somewhat faster than the mean flow speed, a result derived by various authors under slightly different assumptions [44–47].

The effect is due to the fact that the 'tail' of the distribution of $\bar{c}$ is primarily from analyte that is closer to the wall which is lost at a faster rate thereby displacing the centroid forward. Thus, the centroid moves with a velocity that is higher than the mean velocity, $\bar{u}$, but lower than the maximum velociy $u_{max} = 2\bar{u}$. If the adsorption rate $k_a s_m$ is small (which corresponds to our 'slow variations' assumption), the expression for the velocity of the centroid [46, 47] can be linearized with respect to $k_a s_m$. It is then found that the resulting expression is identical to Eq. (55). The same physical effect also brings about a reduction in the effective axial diffusion coefficient. However, the effect is of second order in $k_a s_m$ and is thus not reflected in the expression (50) for $\mathscr{D}$.

The problem of CZE in the presence of wall adsorption is very similar to the problem of open-tubular capillary electrochromatography (CEC) (see, *e.g.*, [48]). However, in CEC the interaction with the wall is an important component of the mechanism of separation rather than an undesirable source of band broadening. In the case of a pressure-driven (Poiseuille) flow, the correction to the migration velocity due to wall interactions, as well as the effective axial diffusion coefficient have been worked out by Golay [44] and later, with greater generality by Aris [45]. In CEC, the flow is electroosmotic rather than pressure-driven. McEldoon and Datta [27] replaced the Poiseuille profile in the Golay-Aris theory by the the Rice-Whitehead flow profile discussed in Section 4 to derive an expression for the dispersion in CEC due to wall interactions. A similar approach has been used earlier by Martin and Guichon [49] and by Martin *et al.* [50], except *ad hoc* approximations to the electrokinetic flow profile were used. The analyte concentration peak profile itself has been calculated numerically recently [51] by integrating a set of one-dimensional model equations. The asymptotic theory presented in this section should also apply to the CEC problem.

6.3 Thermal broadening

The flow of electric current through the buffer in CE systems produces a significant amount of Joule heat which results in temperature variations in the microcapillary. In fact, the problem of Joule heat was a major impediment to the development of CE as an analytical tool. Excessive heating could cause convective overturning in the fluid that would result in obliteration of all signals. The fluid could even vaporize leading to a "vapor lock" and catastrophic failure. These problems were overcome only when microcapillaries (less than 200 μm internal diameter) became available. In modern capillaries or microfluidic channels, Joule heating does not have such disastrous effects, nevertheless it can be a significant source of band broadening.

The transport problem for temperature in a cylindrical capillary carrying a current of uniform density can be easily solved [52] yielding a radially varying temperature field, $T(r)$. The electrophoretic migration speed of molecules varies inversely with the fluid viscosity μ. For example, for a spherical particle with a thin EDL (EDL thickness much less than the particle radius) the Stern-Gouy-Chapman theory [5] gives

$$u_{ep} = \frac{2}{3}\frac{\varepsilon\zeta E}{4\pi\mu} \tag{56}$$

(in cgs units) where ε and μ are the dielectric constant and viscosity of the buffer, E is the applied electric field, and ζ is the zeta-potential at the surface of the migrating particle. Since the viscosity μ varies with temperature, T, which in turn varies with r, analyte molecules near the wall migrate with a slightly different speed than those at the center. This, clearly would lead to band broadening in the sample plug.

How is the EOF modified and what role does it play in the band broadening process? At first sight one might conclude that since the electroosmotic velocity

$$u_{eo} = -\frac{\varepsilon\zeta E}{4\pi\mu} \tag{57}$$

the EOF too should have a profile similar to the electrophoretic velocity. This, however, is not true. The reason is, the formula (57) is valid only for a constant μ not if $\mu = \mu(r)$. If the viscosity depends on r, we must go back to the Stokes equation for determining the correct velocity profile. In the absence of a pressure gradient Stokes equation becomes

$$\frac{1}{r}\frac{\mathrm{d}}{\mathrm{d}r}\left(r\mu(r)\frac{\mathrm{d}u}{\mathrm{d}r}\right) = 0 \tag{58}$$

with the HS slip boundary conditions (in the thin EDL limit):

$$u(r = a_0) = -\frac{\varepsilon\zeta E}{4\pi\mu(a_0)} \tag{59}$$

a_0 being the capillary radius. Assuming that u is not singular at $r = 0$, the unique solution

$$u(r) = u(r = a_0) = -\frac{\varepsilon\zeta E}{4\pi\mu(a_0)} \tag{60}$$

is determined. Thus, the velocity still has a flat profile and the result (57) may still be used, provided that the 'μ' is interpreted as the μ at the wall, $r = a_0$. Thus, it is the modification of the electrophoretic velocity, not the electroosmotic velocity that causes band broadening, as pointed out by Knox [53] who provided the first correct treatment of the thermal band broadening phenomenon. Knox also calculated an explicit expression for the plate height (the variance developed by an initially sharp concentration peak per unit length of capillary traversed by the sample).

A similar analysis was published later by Grushka *et al.* [54] who also provided an expression* for the plate height:

$$H = \frac{2D}{\bar{u}} + \frac{R_1^6 E^4 C_b^2 B^2 \Lambda^2 \bar{u}}{24D\left(8k_1 T_1^2 - E^2 \Lambda C_b R_1^2 B\right)^2} \tag{61}$$

where D is the molecular diffusivity, $\bar{u}$ is the cross-sectionally averaged value for the migration velocity, R_1 is the internal capillary diameter, E is the applied electric field, C_b and Λ are, respectively, the buffer electrolyte concentration and equivalent conductance and k_1 is the buffer thermal conductivity. Finally, the coefficients A and B characterize the temperature dependance of the viscosity of the buffer: $\mu = A \exp(B/T)$, T being the absolute temperature and T_1 its value at the wall. Andreev and Lisin [55] analyzed the problem by numerically solving the coupled equations for Stokes flow, the Poisson-Boltzmann equation for the electric potential, and the advection diffusion equation for the analyte concentration taking into account the dependence of the transport coefficients on concentration and temperature. The thermal equation was integrated analytically assuming a small temperature drop between the axis and the wall of the capillary, which implies a parabolic distribution of the temperature profile. It was found that depending on the parameter regime, the effect of the nonuniform temperature on the EOF could sometimes dominate effects due to variations of the electrophoretic velocity. This is due to the finite Debye layer effects which disappear in the thin EDL limit considered by Knox [53] and by Grushka *et al.* [54].

The wall temperature can be calculated by solving the steady state diffusion equation with a source. This has been done by various authors under different assumptions. Grushka *et al.* [54] assume a polyimide-coated capillary and constant electrical and thermal conductivity of the buffer, in which case

$$T_1 = T_a + \frac{GR_1^2}{2}\left[\frac{1}{k_2}\ln\left(\frac{R_2}{R_1}\right) + \frac{1}{k_c}\ln\left(\frac{R_c}{R_2}\right) + \frac{1}{R_c h}\right] \tag{62}$$

where T_a is the ambient temperature, h is the heat transfer coefficient to the surroundings (power radiated per unit area per unit temperature difference between the outer

* The author's expression for what they call the "electrophoretic migration velocity" appears to be missing a pre-factor (2/3 for spherical particles with thin EDL), however, this should not affect the final result, Eq. (61) which depends only on the fact that this velocity is inversely proportional to the viscosity.

wall and the environment), R_c and R_2 are the outer capillary diameters with and without the polyimide coating, k_2 and k_c are the thermal conductivities of fused-silica and polyimide coating, respectively, and G is the (constant) heat generation rate. The temperature distribution within the buffer itself has a parabolic profile. A more accurate model for calculating the temperature distribution must account for the variation of buffer electrical conductivity with temperature. In that case the heat generation rate is no longer constant but to a good approximation a linear function of temperature. The resulting equation for thermal transport is nevertheless still linear, and may be readily solved in terms of the zeroth order Bessel function [56]. However, as shown by Jones and Grushka [56], under typical CE operating conditions the correction to the parabolic temperature profile obtained assuming constant conductivity is very small.

In addition to the obvious radial dependence on temperature, axial variations in temperature could also occur due to various inhomogeneities in the capillary. Such variations could induce pressure gradients and lead to band broadening. It is not clear whether such axial variations are present and if so whether they do cause significant dispersion. Convective motion of fluid in the capillary is also possible. These are open areas for investigation.

6.4 Dispersion in curved channels

In a typical laboratory CE unit the capillary is usually straight, or has a radius of curvature very much larger than the capillary diameter (in which case it may be considered essentially straight). However, for CE systems, the requirement of a long analysis section (in order to support a larger voltage drop, the number of theoretical plates being proportional to the voltage drop) forces one to consider sinuous channels in order to fit it on a chip of modest footprint.

Such curved channels contribute to axial dispersion due to the following mechanism: Since the isopotential surfaces intersect the channel boundaries at right angles (ignoring the finite thickness of the EDL) the same potential drop occurs over a shorter distance on the inner side of a curve than on the outer side. As a result, the applied voltage creates a stronger field on the inside edge of the channel. Therefore, by the HS slip boundary condition, the fluid velocity is higher at the inner edge than at the outer one. Further, solute particles near the inner edge of the turn traverse a shorter distance at this higher speed than particles at the outer edge (the so-called "race track effect"). Thus, as a band goes round the bend it is sheared out of shape. Cross-stream molecular diffusion acts on this shear resulting in an enhanced effective axial dispersion due to the Taylor-Aris mechanism. Minimizing such turn induced "geometric dispersion" is a subject of active research interest (see, *e.g.*, the short report by Zubritsky [57] for an overview of the approaches being pursued).

The simplest geometry is that of a rectangular channel of width '*a*' and infinite depth that has a curved region with a turn angle of θ (in radians) connecting infinitely long inlet and outlet sections. The channel is assumed to lie in a single plane. The following formula has been proposed by Griffiths and Nilson [28] for the turn induced axial variance σ^2:

$$\left(\frac{\sigma}{a}\right)^2 = \frac{\theta^2 Pe}{15r_* + 3Pe} + \frac{2r_*\theta}{Pe} \tag{63}$$

Here, r_* is the mean of the radii of curvature of the inner and outer walls normalized by the channel width, and $Pe = aU/D$ is the Peclet number based on the (uniform) flow speed far upstream of the bend (U) and the molecular diffusion coefficient (D).

There are two qualitatively different regimes of interest. The distinction is based on whether the cross stream diffusion of species is dominant or if it is a small correction. The characteristic time scale required for any concentration variation across the channel to be homogenized is $t_D \sim a^2/D$. This is to be compared with the characteristic residence time of the sample in the curved section of the capillary, $t_R \sim ar_*\theta/U$. Clearly if $t_A \ll t_D$ diffusion is unimportant and the dispersion may be calculated from purely geometrical considerations. The ratio

$$t_A/t_D \sim r_*\theta/Pe \tag{64}$$

Thus, we distinguish between the (i) Low Peclet number regime: $t_A/t_D \gg 1$ which corresponds to turns of relatively large radius of curvature or large diffusion coefficients. In this case, cross-stream diffusion is dominant so that the concentration is almost constant across the capillary. Thus, the variance may be obtained through a straight forward substitution of the analytical expression for the velocity profile in the Taylor-Aris formalism for calculating the variance. (ii) High Peclet number regime: $t_A/t_D \ll 1$ which corresponds to small radius of curvature and low molecular diffusion coefficients. In this case, the dispersion may be calculated by purely geometrical means since the solute is simply advected along streamlines.

The expression (63) is an empirically constructed "composite expression" that reduces to the correct limits in the low and high Peclet number regimes. In these two limits the expression (63) for the variance take the following forms

$$\sigma^2 \sim \left[2D + \frac{\bar{u}^2 a^4 \theta}{15\bar{r}^2 D}\right] t_A \ (Pe \to 0) \tag{65}$$

$$\sigma^2 \sim \frac{\theta^2 a^2}{3} + 2Dt_A \ (Pe \to \infty) \quad (66)$$

where $\bar{r} = ar_*$ is the dimensional mean radius of curvature and $t_A = \bar{r}\theta/U$ is the transit time across the bend. The former expression clearly has the form of the variance due to molecular diffusion added to a Taylor-like term. In the second case we have molecular diffusion plus a purely geometrical quantity that is independent of the diffusion coefficient D but depends solely on the difference of path lengths $a\theta$ between the inner and outer edges of the bend. In microfluidic applications both limits are relevant. For example, if we take $a \sim 100$ μm, $\bar{r} \sim 1$ cm and $\theta = \pi$ then $r_*\theta \sim 300$. Since $Pe \sim 10^1 - 10^2$ for small molecules but $Pe \sim 10^3 - 10^4$ for macromolecules it is clear from Eq. (64) that the 'high' the 'low' as well as the 'intermediate' Peclet number regimes are relevant for microfluidic applications. Culbertson *et al.* [58] also considered the problem of geometric dispersion in a rectangular channel undergoing a 180° turn. They used an *ad hoc* modification of the expression for the axial stretching of an initially sharp bend in the absence of diffusion to incorporate diffusive effects. The model was fitted to experimental data. However, their model differs from Eq. (63) by a numerical factor at low Peclet numbers and the apparent agreement with experimental data in this regime has been attributed by Griffiths and Nilson [28] to uncertainties in the measurement of the channel width.

The first term in Eq. (63) increases linearly with *Pe* for small values of *Pe* and saturates at large *Pe*. Clearly the dispersion contribution from this term can be reduced if either *Pe* can be reduced or else if r_* could be increased. Two main ideas for designing low dispersion bends have evolved out of these two possibilities. The channel can be 'pinched' so that it becomes very narrow in the curved sections. This effectively reduces the *Pe* locally by decreasing *a*. This approach has been investigated by Paegel *et al.* [59]. Alternatively one could design the separation channel in the form of spiral turns of large radii of curvature. This approach, which relies on increasing the effective radius of curvature r_*, has been followed, for example, by Culbertson and others [60–62]. Yet a third possibility is to redesign the channel geometry at the bend so as to compensate for both the higher electric field and the 'race track' effect. Effectively this is equivalent to attempting to reduce the prefactor multiplying the *Pe* in the first term of Eq. (63) by altering the velocity distribution. This approach has been adopted for example by Molho *et al.* [63, 64] who tried to come up with optimal shapes using computer simulation. The results were compared to experimental data and appeared to show reasonable agreement. Similar designs were proposed by Griffiths and Nilson [65]. Others have attempted to combine several of these ideas. For example, Dutta and Leigton have proposed spirals with inner walls that are wavy to compensate for the shorter path [66] thereby both increasing r_* as well as reducing the geometric prefactor in (63). Johnson *et al.* [67] achieve the same effect by modifying the wall ζ-potential through laser ablation, which will also change the pattern of EOF in the channel. Fiechtner and Cummings [68] have proposed a 'faceted' design which is a polygonal shape approximating a smooth spiral. Griffiths and Nilson [69] have investigated 'pleated channels' where some of the turn induced dispersion is 'undone' at the following turn in the opposite direction.

7 Summary and conclusions

Electroosmosis and electrophoresis are closely related phenomena which are often present together in CZE. EOF is an effect of the action of the applied electric field on the Debye layer of free charges adjoining the walls of a microfluidic channel. Electroosmosis is both an ally and an enemy of the researcher interested in achieving efficient separation. The main advantage of EOF is that it is a useful means for transporting analytes and buffer in a microfluidic circuit. Unlike pressure-driven flows in which the pressure drop needed to maintain a certain fixed mean flow speed increases inversely as the square of the capillary radius, in EOF, the voltage needed is independent of the capillary radius. Thus, EOF is very efficient for transporting infinitesimal volumes of fluid through very narrow capillaries. The presence of EOF in the microchannels enables single point detection (species of either sign elute at the same end), reduces analysis times and enables operation of the microdevice in a continuous mode. The disadvantage is that any effect that causes the EOF flow profile to deviate from the classical "plug flow" shape would cause band broadening.

The state of current knowlege of the fluid mechanics of EOF was reviewed with special attention to the role of EOF on dispersion in CZE systems. EOF is fully described by the Poisson-Boltzmann equation coupled to the incompressible Navier-Stokes and continuity equations describing fluid flow. This set of equations is, however, quite complex and nonlinear, exact analytical solutions can be found only for certain highly idealized systems. Fortunately, however, a series of simplifications can be made to these equations, at each step exploiting a certain disparity in scales inherent in the problem.

The first level of simplification comes about through the assumption of thin Debye layers. This is justified, since in most current applications to EOF, characteristic channel radii are of the order of 10–100 μm whereas for the normal

range of buffer concentrations used, the Debye length is 1–10 nm. This disparity in scales allows us to drop the term representing the electrical force in the Navier-Stokes equations and instead, to replace the classical "no slip" boundary conditions at the solid fluid interface by the "HS slip boundary conditions". Thus, within the realm of this approximation, the electrical forces are described by a single parameter, 'the ζ-potential' that enters the fluid flow description solely through the new 'slip' boundary conditions and the Poisson-Boltzmann equation may be replaced by the Laplace equation for a charge free region.

If fluid properties and the ζ-potential are uniform, no external pressure gradient is applied, the substrate is a poor electrical conductor and the Reynolds number is negligibly small, then the fluid velocity through a channel of any geometry is simply proportional to the electric field which may be determined by solving a Dirichlet problem for the electric potential. This 'similitude' between the electric field and the hydrodynamic flow also applies to the finite Reynolds number situation provided the flow is irrotational. However, the assumption of uniform fluid properties and ζ-potential is not valid in all problems of interest, such as in the problem of flow modification due to wall interactions.

In such cases an alternate approximation becomes possible due to the smallness of channel diameters (10–100 μm) compared to overall capillary length (10–100 cm). This allows us to invoke a well developed branch of fluid mechanics, namely "lubrication theory" for the description of the fluid flow. The consequent reduction in complexity enables a rational description of an important class of problems involving EOF; namely the problem of EOF through channels that are not homogeneous in the axial direction. Axial inhomogeneity can arise due to a variety of reasons, in particular due to adsorption of charged sample components to the wall (which in turn changes the ζ-potential), variations in temperature due to nonuniform heating or cooling, alteration of the electrical conductivity of the buffer by the sample or axial variation in buffer pH (as in sample stacking or isoelectric focusing).

One of the most important results of flow modification in CZE is its effect on the effective axial dispersion of the analyte. Here, the basic fluid mechanics tool at our disposal is the "Taylor-Aris dispersion theory" for the long time evolution of a scalar field in a shear flow and the various generalizations and modifications of it that have been developed over the years. Axial dispersion or band broadening arises out of three main sources: (i) axial inhomogeneities, (ii) radial inhomogeneities, and (iii) channel curvature. In general, axial inhomogeneities of any kind lead to an induced axial pressure gradient due to the incompressibility constraint. Such pressure fluctuations give rise to a "Poiseuille" type of flow with a parabolic profile, which through the mechanism of Taylor-Aris dispersion leads to greatly enhanced effective axial dispersion. Radial variations are often caused by nonuniform temperature distributions inside the capillaries and cause band broadening due to differential rates of electromigration over the capillary cross-section. Channel curvature results in 'geometric dispersion' and is relevant at the low, intermediate as well as high Peclet number regimes.

Though the basic analytical machinery for treating EOF in a wide variety of situations of interest appear to be available, there are many areas where theoretical understanding is in a relatively primitive state. Advances in the study of this new area of fluid mechanics should facilitate the development of software and numerical tools that could be very useful in the quest to develop μ-TAS technology and more efficient separation methods.

Received August 18, 2003

8 References

[1] Reuss, F. F., *Mémoires de la Societé Impériale des Naturalistes de Moscou* 1809, *2*, 327–337.

[2] Probstein, R., *Physicochemical Hydrodynamics*, John Wiley and Sons, New York 1994.

[3] Taylor, G. I., *Proc. Roy. Soc. A* 1953, *219*, 186–203.

[4] Aris, R., *Proc. Roy. Soc. A* 1956, *235*, 67–77.

[5] Russel, W. B., Saville, D. A., Schowalter, W. R., *Colloidal Dispersions*, Cambridge University Press, Cambridge, UK 1989.

[6] Anderson, J. L., *J. Coll. Int. Sci.* 1985, *105*, 45–54.

[7] Helmholtz, H. von, *Ann. Physik Chemie* 1879, *7*, 337–387.

[8] Smoluchowski, M. von, *Bull. Int. Acad. Sci. Cracovie* 1903, *8*, 182–200.

[9] Rice, C. L., Whitehead, R., *J. Phys. Chem.* 1965, *69*, 4017–4024.

[10] Abramowitz, M., Stegun, I. A. (Eds.), *Handbook of Mathematical Functions*, Dover Publications, New York, USA 1970.

[11] Burgreen, D., Nakache, F. R., *J. Phys. Chem.* 1964, *68*, 1084–1091.

[12] Anderson, J. L., Idol, W. K., *Chem. Eng. Commun.* 1985, *38*, 93–106.

[13] Ajdari, A., *Phys. Rev. Lett.* 1995, *75*, 755–758.

[14] Ajdari, A., *Phys. Rev. E* 1996, *53*, 4996–5005.

[15] Stroock, A. D., Weck, M., Chiu, D. T., Huck, W. T. S., Kenis, P. J. A., Ismagilov, R. F., Whitesides, G. M., *Phys. Rev. Lett.* 2000, *8415*, 3314–3317.

[16] Anderson, J. R., McDonald, J. C., Stone, H. A., Whitesides, G. M., preprint.

[17] Long, D., Stone, H. A., Ajdari, A., *J. Coll. Int. Sci.* 1999, *212*, 338–349.

[18] Cummings, E. B., Griffiths, S. K., Nilson, R. H., Paul, P. H., *Anal. Chem.* 2000, *72*, 2526–2532.

[19] Batchelor, G., *An Introduction to Fluid Dynamics*, Cambridge Univ. Press, Cambridge, UK 2000.

[20] Lighthill, M. J., *J. Fluid Mech.* 1968, *34*, 113–143.
[21] Secomb, T. W., Skalak, R., Özkaya, N., Gross, J. F., *J. Fluid Mech.* 1986, *163*, 405–423.
[22] Ghosal, S., *J. Fluid Mech.* 2002, *459*, 103–128.
[23] Gaš, B., Kenndler, E., *Electrophoresis* 2000, *21*, 3888–3897.
[24] Gaš, B., Štědrý, M., Kenndler, E., *Electrophoresis* 1997, *18*, 2123–2133.
[25] Datta, R., Kotamarthi, V. R., *AIChE J.* 1990, *36*, 916–926.
[26] Griffiths, S. K., Nilson, R. H., *Anal. Chem.* 1999, *71*, 5522–5529.
[27] McEldoon, J. P., Datta, R., *Anal. Chem.* 1992, *64*, 227–230.
[28] Griffiths, S. K., Nilson, R. H., *Anal. Chem.* 2000, *72*, 4767–4777.
[29] Gaš, B., Štědrý, M., Kenndler, E., *J. Chromatogr. A* 1995, *709*, 63–68.
[30] Bonvent, J. J., Bartolino, B. R., Capelli, L., Righetti P. G., *Electrophoresis* 1996, *756*, 233–43.
[31] Ghosal, S., *J. Fluid Mech.* 2003, *419*, 285–300.
[32] Doherty, E. A. S., Meagher, R. J., Albarghouthi, M. N., Barron, A. E., *Electrophoresis* 2003, *24*, 34–54.
[33] Gaš, B., Štědrý, M., Rizzi, A., Kenndler, E., *Electrophoresis* 1995, *6*, 958–967.
[34] Štědrý, M., Gaš, B., Kenndler, E., *Electrophoresis* 1995, *16*, 2027–2033.
[35] Ermakov, S. V., Zhukov, M. Y., Capelli, L., Righetti, P. G., *J. Chromatogr. A* 1995, *699*, 297–313.
[36] Schure, M. R., Lenhoff, A. M., *Anal. Chem.* 1993, *65*, 3024–3037.
[37] Zhukov, M. Y., Ermakov, S. V., Righetti, P. G., *J. Chromatogr. A* 1997, *766*, 171–185.
[38] Towns, J. K., Regnier, F. E., *Anal. Chem.* 1992, *64*, 2473–2478.
[39] Herr, A. E., Molho, J. I., Santiago, J. G., Mungal, M. G., Kenny, T. W., Garguilo, M. G., *Anal. Chem.* 2000, *72*, 1053–1057.
[40] Ghosal, S., *Anal. Chem.* 2002, *74*, 771–775.
[41] Ghosal, S., *Anal. Chem.* 2002, *74*, 4198–4203.
[42] Shariff, K., Ghosal, S., *Anal. Chim. Acta* 2003, in press.
[43] Bruin, G., Huisden, R., Kraak, J., Poppe, H. J., *J. Chromatogr.* 1989, *480*, 339–349.
[44] Golay, M. J. E., *Contribution to the Gas Chromatography Symposium*, Amsterdam 1958.
[45] Aris, R., *Proc. Roy. Soc. A* 1959, *252*, 538–550.
[46] Lungu, E. M., Moffatt, H. K., *J. Engg. Math.* 1982, *16*, 121–136.
[47] Sankarasubramanian, R., Gill, W. N., *Proc. R. Soc. A* 1973, *333*, 115–132.
[48] Weinberger, R., *Practical Capillary Electrophoresis*, Academic Press, New York 2000.
[49] Martin, M., Guiochon, G., *Anal. Chem.* 1984, *56*, 614–620.
[50] Martin, M., Guiochon, G., Walbroehl, Y., Jorgenson, J. W., *Anal. Chem.* 1985, *57*, 559–561.
[51] Pačes, M., Kosek, J., Marek, M., Tallarek, U., Seidel-Morgenstern, A., *Electrophoresis* 2003, *24*, 380–389.
[52] Burgi, D. S., Salomon, K., Chien, R. L., *J. Liq. Chromatogr.* 1991, *14*, 847–867.
[53] Knox, J. H., *Chromatographia* 1988, *26*, 329–337.
[54] Grushka, E., McCormick, R. M., Kirkland, J. J., *Anal. Chem.* 1989, *61*, 241–246.
[55] Andreev, V. P., Lisin, E. E., *Electrophoresis* 1992, *13*, 832–837.
[56] Jones, A. E., Grushka, E., *J. Chromatogr.* 1989, *466*, 219–225.
[57] Zubritsky, E., *Anal. Chem.* 2000, *72*, 687A–690A.
[58] Culbertson, C. T., Jacobson, S. C., Ramsey, J. M., *Anal. Chem.* 1998, *70*, 3781–3789.
[59] Paegel, B. M., Hutt, L. D., Simpson, P. C., Mathies, R. A., *Anal. Chem.* 2000, *72*, 3030–3037.
[60] Culbertson, C. T., Jacobson, S. C., Ramsey, J. M., *Anal. Chem.* 2000, *72*, 5814–5819.
[61] Miyahara, Z. Y., Miura, J., Watanabe, Y., Miyagi, H., Sato, K., *Sens. Actuators B1* 1990, 249–255.
[62] Gottschlich, N., Jacobson, S. C., Culbertson, C. T., Ramsey, J. M., *Anal. Chem.* 2001, *73*, 2669–2674.
[63] Molho, J. I., Herr, A. E., Mosier, B. P., Santiago, J. G., Kenny, T. W., *Anal. Chem.* 2001, 73, 1350–1360.
[64] Mohammadi, B., Molho, J. I., Santiago, J. G., in: Moin, P., Reynolds, W. C., Mansour, N. N. (Eds.), *Studying Turbulence Using Numerical Simulation Databases – VIII, Proceedings of the 2000 Summer Program*, Center for Turbulence Research, Stanford University, Stanford, CA 2000, pp. 49–62.
[65] Griffiths, S. K., Nilson, R. H., *Anal. Chem.* 2001, *73*, 272–278.
[66] Dutta, D., Leighton, D. T., *Anal. Chem.* 2002, *74*, 1007–1016.
[67] Johnson, T. J., Ross, D., Gaitan, M., Locascio, L. E., *Anal. Chem.* 2001, 73, 3656–3661.
[68] Fiechtner, G. J., Cummings, E. B., *Anal. Chem.* 2003, *75*, 4747–4755.
[69] Griffiths, S. K., Nilson, R. H., *Anal. Chem.* 2002, *74*, 2960–2967.